Check for updates

Productive preparation of N-doped carbon dots from sodium lignosulfonate/melamine formaldehyde foam and its fluorescence detection of trivalent iron ions

Yong-Yan Pan,†[a] Wei-Ming Yin, [ID] †[a] Ran-Jun Meng,[a] Yuan-Ru Guo, [ID] *[a] Ji-Guo Zhang*[a] and Qing-Jiang Pan [ID] *[b]

Due to its good properties and low cost, melamine formaldehyde foam has been widely used in cars, furniture and construction. However, how to recycle the spent foam still remains challenging for scientists. In this work, a new method was designed to prepare N-doped carbon dot (NCD) materials by calcining sodium lignin sulfonate/melamine formaldehyde foam (LSMF) via one step. TEM, IR and XPS were used to characterize the structure and morphology of newly-synthesized NCDs. It is shown that carbon powder is obtainable by calcination. Since it derives from the collapse of the foam structure of LSMF, the carbon powder can almost completely dissolve in deionized water. The particle size ranges from 5 to 20 nm. The fluorescence properties of NCDs were studied by fluorescence spectroscopy. A strong emission has been detected at 580 nm with the quantum yield of 2.94%. When applying NCDs to detect various metal ions, there is a significant fluorescence quenching effect and good selectivity for Fe^{3+}. The mechanism has been hypothesised. Our study provides a method for productive preparation of NCDs from spent foam.

Introduction

Environmental pollution is a major issue in the 21st century.[1,2] How to efficiently use existing resources and achieve "turning waste into treasure" is the research goal of many researchers.[3] Melamine formaldehyde foam (MF) is a thermosetting polymer foam with excellent flame retardancy and high corrosion resistance. Because of its high porosity and sound insulation and thermal insulation properties, MF is widely used in the construction industry.[4,5] In order to use the environmentally friendly MF, many methods have been applied for its preparation. For example, Zhang *et al.*[6] prepared a new type of micro-encapsulated phase change material using paraffin wax as the core and hydrophobic silicon carbide modified MF resin as the shell. The uniform distribution of H–SiC on the surface of the microcapsules has an effect on the heat conduction and heat dissipation of the microcapsules. In the work of Zhu *et al.*,[7] ethylene glycol was used to modify MF resin, and the product

was made to a filler; further association with polyols and poly-isocyanates prepared rigid polyurethane foams.

However, how to prepare MF in an environmentally friendly route or how to reuse MF to achieve the "sustainable" development is still a problem for scientists to face with. Some strategies have been adopted to fulfil this goal, for instance, using bioresource lignin. Lignin, as the second largest natural polymer on earth, was applied to produce MF, which reduced the addition of formaldehyde. Compared with other biopolymers, lignin has the advantages of biocompatibility as well as high carbon content.[1,8] The introduction of lignin can reduce the production cost of MF and the release amount of formaldehyde. However, it can't solve the recycle problem of spent foam. More work is encouraged to work on this aspect.

Iron ion, Fe^{3+} for instance, is one of the indispensable trace elements in human life. The recommended intake of iron ranges from 8 to 18 mg per day for normal adult. But excessive intake of iron will cause iron poisoning.[9] Moreover, Fe^{3+} cannot be metabolized in the human body, which can lead to serious liver and kidney damage and even death.[10] Carbon dots (CDs) are soluble and fluorescent nanoparticles, which were firstly reported by Xu *et al.*[11] As a new type of zero-dimensional nanomaterial, CDs bears a graphite phase core, and its surface is full of hydrophilic groups such as hydroxyl and carboxyl groups,[12–14] which bring the fascinating property of CDs. CDs has been applied as fluorescence sensor for detecting

[a]*Key Laboratory of Bio-based Material Science & Technology (Ministry of Education), Material Science and Engineering College, Northeast Forestry University, Harbin 150040, China. E-mail: guoyrnefu@163.com; 116920813@qq.com*

[b]*Key Laboratory of Functional Inorganic Material Chemistry (Ministry of Education), School of Chemistry, Chemical Engineering and Materials, Heilongjiang University, Harbin 150080, China. E-mail: panqjitc@163.com*
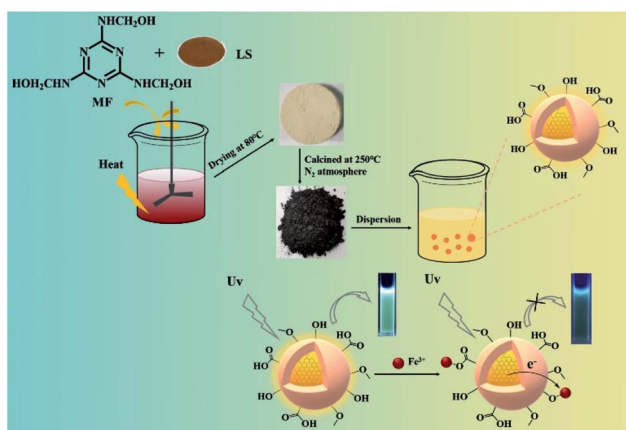
† The two authors equally contributed to this work.

various metal ions due to the abundant active sites on its surface.[15]

Taking advantage of the rich carbon source of waste foam, we used a one-step calcination method to prepare nitrogen doped carbon dots (NCDs) from sodium lignosulfonate/ melamine formaldehyde foam (LSMF). The newly-obtained NCDs show intensive fluorescence and preferential detection performance on iron ion over other common s/d-block metal ions. The synthetic route and testing has been shown in Scheme 1. The work provides a reasonable solution to the problem of recycling of waste LSMF and achieves the purpose of rational utilization of resources.

Results and discussion

In order to study the structure of materials before and after sintering, XRD was performed and result is shown in Fig. 1a. It can be seen that LSMF has a broad peak at 19–26°, indicating that LSMF is an amorphous polymer material. However, a relative sharp peak near $2\theta = 25.6°$ was observed after calcination, which is corresponding to the (002) plane of graphite carbon.[16–18] The change of XRD plots shows that the LSMF has transformed into carbon material.

IR was also applied to study the functional groups of both LSMF and NCDs, as shown in Fig. 1b. To LSMF, the main absorption bands of LSMF at 1450–1600 cm^{-1} correspond to the triazine ring, and the absorption peak at 2898 cm^{-1} is vibration of $-CH_2/-CH_3$. The peaks around 3100 and 3300 cm^{-1} are $-OH$ and $-NH$ vibration. Due to large molecular skeleton, these two peaks connected to each other and formed a broad peak. To the IR spectrum of NCDs, these two peaks are totally separated. Moreover, the intensity of $-OH$ was enhanced, which indicated that more $-OH$ groups found on NCDs. Meanwhile, multiple peaks are found in functional group region, peaks at 1641 cm^{-1} are vibration of C=C group of the aromatic ring, the absorption peaks at 1380 cm^{-1} and 1331 cm^{-1} are derived from the stretching vibration of C–N, peaks at 1499 cm^{-1} are the flexural vibration absorption peaks of sp^2 hybrid C framework. The absorption peak at 1037 cm^{-1} is related to the C–O–C ether bond.
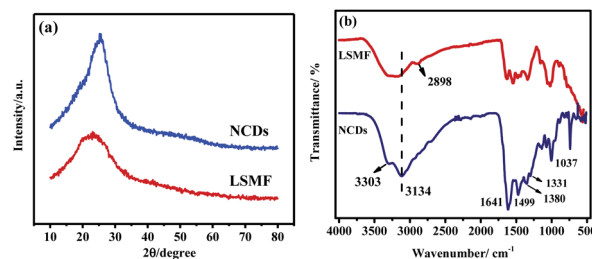

Fig. 1 The XRD patterns (a) and FT-IR spectra (b) of the LSMF and NCDs.

SEM is applied to characterize the morphology of both LSMF and NCDs. It can be seen in Fig. 2a and b that LSMF foam is constructed by hollow ball, which has diameter about 2.5 μm. And these balls connected to each other and form the network. The hollow spherical structure of foam makes it excellent thermal insulation material on one hand, it also makes itself easy to be decompose to CDs on the other hand. After treated at 250 °C, the foam structure collapsed and pieces of carbon can be obtained as can been seen in Fig. 2c and d. Though CDs was formed at this stage, these CDs are still clustered together and maintaining a collapsed cross-linked structure. Once dissolved in distilled water and ultrasound treated for 30 min, almost all the carbon dissolved into water and result in yellow solution. This gives the evidence that carbon dots can been prepared by simply heated the LSMF at 250 °C by solid reaction. Since there are abundant of C–OH, C–N–H and C=O functional groups on the surface, the prepared NCDs shows high solubility. After centrifugation and removal of the residue, a yellow transparent NCDs solution can be obtained.

TEM was applied to further analyse the structure of NCDs and the results are shown in Fig. 3. It can be seen that the NCDs we prepared has good dispersibility, and the particle size ranges from 5 to 20 nm. In the high-resolution image, clear lattice

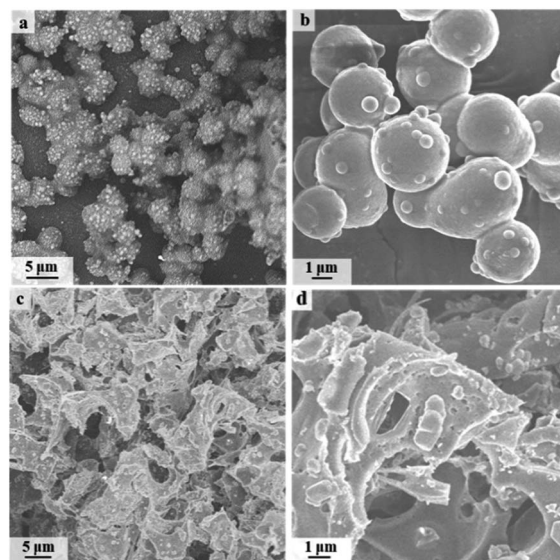Scheme 1 Preparation of NCDs and quenching effect by Fe^{3+} ions.

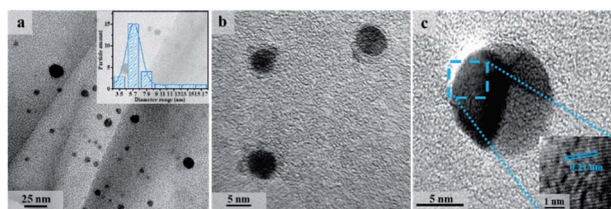Fig. 2 SEM images LSMF (a and b) and NCDs (c and d).

Fig. 3 TEM images of NCDs (a and b), along with the HRTEM image (c).

fringes can be found with the crystal plane spacing of 0.21 nm, which corresponds to the (002) crystal plane of graphite. Combined with infrared analysis results, the prepared NCDs have sp^2 hybrid graphite cores.

XPS was applied to explore the doping elements in NCDs and their chemical environment, as shown in Fig. 4. According to XPS analysis, NCDs mainly contain C, O, N elements. Fig. 4a is C 1s spectrum of NCDs. It is fitted to five peaks with binding energies of 284.4, 285.2, 286.7 and 288.2 eV. The first peak belongs to the C–C bond, which indicates that the prepared NCDs contains the sp^2 hybrid graphite carbon phase. The following two correspond to binding energies of C–H and O–C=O, respectively. And the last peak at 288.2 eV indicates the existence of C–O bond. The O 1s spectrum (Fig. 4b) can be fitted for four peaks at 530.5, 531.5, 532.3 and 533.3 eV, which are assigned to C–O, O–H, C–O–C and O–C=O, respectively. The relative strong peaks also give the evidence that there are plenty of oxygen containing functional groups on NCDs. The spectrum of N 1s has peaks at binding energy of 397.6, 398.4 and 399.4 eV (see Fig. 4c), which are related to C≡N, C–N and N–H, respectively.

According to the XPS results, during the preparation of NCDs by solid-phase sintering, new functional groups were introduced on the surface of NCDs. These functional groups provided fluorescence emission centres for NCDs, which matched the results of the subsequent fluorescence spectrum analysis.

In order to explore the fluorescence properties of the prepared NCDs, both ultraviolet spectroscopy and fluorescence spectroscopy were used to characterize NCDs. Fig. 5a shows the scan results of the UV and fluorescence spectra of NCDs. According to the literature,[15,19] the absorption peaks of NCDs at 212 nm and 251 nm are caused by the π–π* transition originated from sp^2 hybridized C. A adsorption with relatively low intensity around 280–300 nm, which is mainly caused by the n–π* transition of C=O/C–N. Generally, the fluorescence emission mechanism of CDs mainly involves three aspects: the size
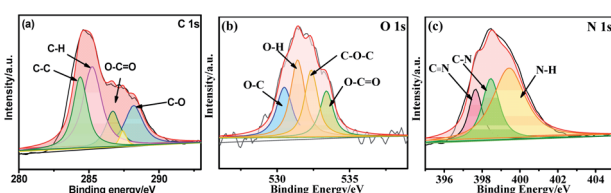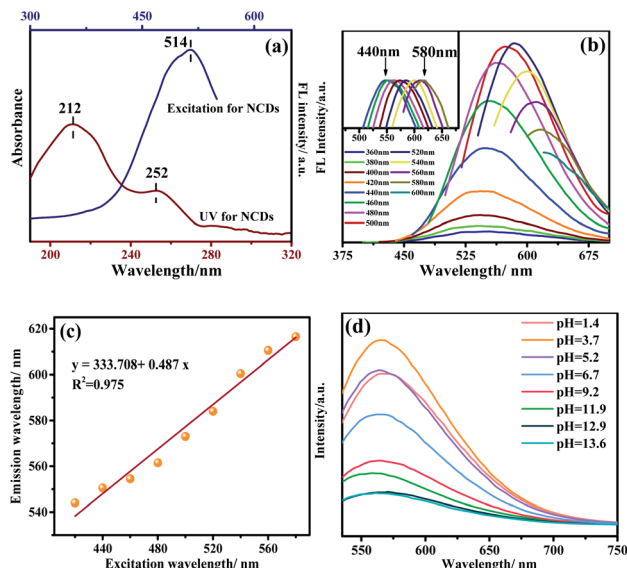

Fig. 5 UV-Vis and fluorescence spectra of NCDs (a), fluorescence spectra excited by various wavelengths (b), and the insert picture is the plot after normalization, the linear correlation plot of excitation *versus* emission (c) and fluorescence spectra while varying solution pH value (d).

effect of CDs, the electronic transition of sp^2 hybrid carbon nuclei, and the surface passivation.[20]

The fluorescence excitation spectrum of NCDs is also shown in Fig. 5a. It can be seen that NCDs have the strongest fluorescence emission peak under excitation at 514 nm. Since the strongest emission of CDs may affect by excitation wavelength, the emission spectra of NCDs at different excitation wavelengths were also performed. As shown in Fig. 5b and c, the emission of NCDs has a significant red shift with the increase of excitation wavelength. The "excitation wavelength dependence" phenomenon occurs due to the complex surface state of NCDs: the dominant emission site on the surface of NCDs changes accordingly and lead to different emission wavelengths when excited at different excitation wavelengths.[21] Calcination process makes the surface of the CDs passivated on one hand, on the other hand it produced abundant functional groups, which improved the fluorescence performance. Meanwhile, the N element was introduced into CDs, which increase the defect energy level on the surface of NCDs, and promote NCDs fluorescence intensities. Meanwhile, the fluorescence quantum yield of NCDs was determined to be 2.94% using the photoluminescence spectrometer.

To consider the pH effect, the fluorescence intensity was determined in the solution of different pH values. The results are presented in Fig. 5d. One can see that the NCDs exhibits the strongest intensity at pH = 3.74. Starting from it, higher pH solution affords lower fluorescence intensity. It can be attributed to the presence of more hydroxyl functional groups on the NCDs. It is known that the bonding of the hydroxyl groups to NCDs destroys the π conjugation of carbon dots and eventually lowers the transition possibility of π* → π.

Due to its good fluorescent property, the application of as NCDs as fluorescent probe to detect metal ions were also carried

Fig. 4 XPS curves of NCDs, C 1s (a), O 1s (b) and N 1s (c).

out the fluorescence intensity of the aqueous solution of NCDs before and after mixed with metal ions (μmol L^{-1}) were measured by a fluorescence spectrometer and the result is shown in Fig. 6a and b. According to the results NCDs solution gives cyan-green colour. After interacting with metal ions, the fluorescence intensity of mixture decreases and colour changes to blue except of Fe^{3+}. Fe^{3+} has the most obvious fluorescence quenching effect in NCDs solution. The quenching effect is also can been observed under ultraviolet light irradiation (Fig. 6b). This gives the evidence that Fe^{3+} can be identified from other metals ions by our NCDs.

The fluorescence quenching mechanism of Fe^{3+} toward NCDs was also explored by adding 15 μL Fe^{3+} ions to 3 mL NCDs solution. The concentration of Fe^{3+} ion varies from 9, 18, 35, 45, 90, 180, 360 to 450 μmol L^{-1}. Both Stern–Volmer (eqn (1)) and double logarithmic regression model (eqn (2)) were used to analyse the quenching mechanism.[22,23] Results are shown in Fig. 7a and b.

$$F_0/F = 1 + K_{sv}Q \tag{1}$$

$$\log(F_0/F - 1) = \log K + n\log Q \tag{2}$$

where the fluorescence intensity of NCDs and the mixture (NCDs and Fe^{3+}) corresponds to F_0 and F, Q is the concentration of metal ion quencher, K is the binding constant, and n reflects the number of binding sites for static quenching.

Generally, the fluorescence quenching mechanism involves dynamic quenching, static quenching[24,25] and internal filtration
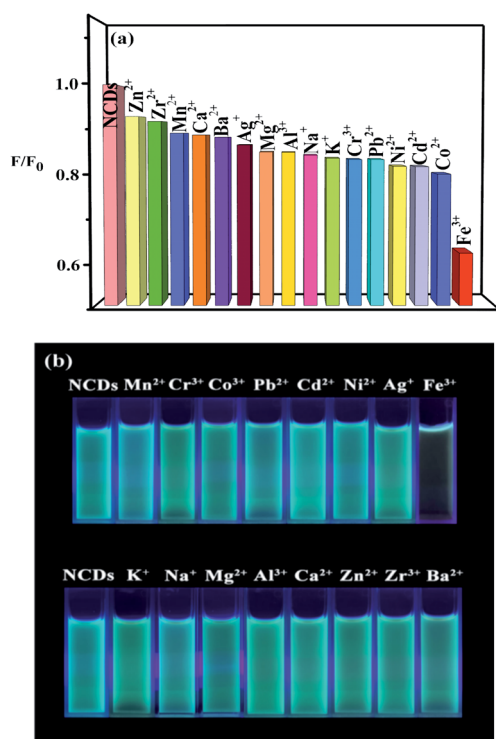

Fig. 6 Quenching selectivity of NCDs for different metal ions, the relative fluorescence intensities (a) and the taken pictures illuminated under the 365 nm UV light (b).
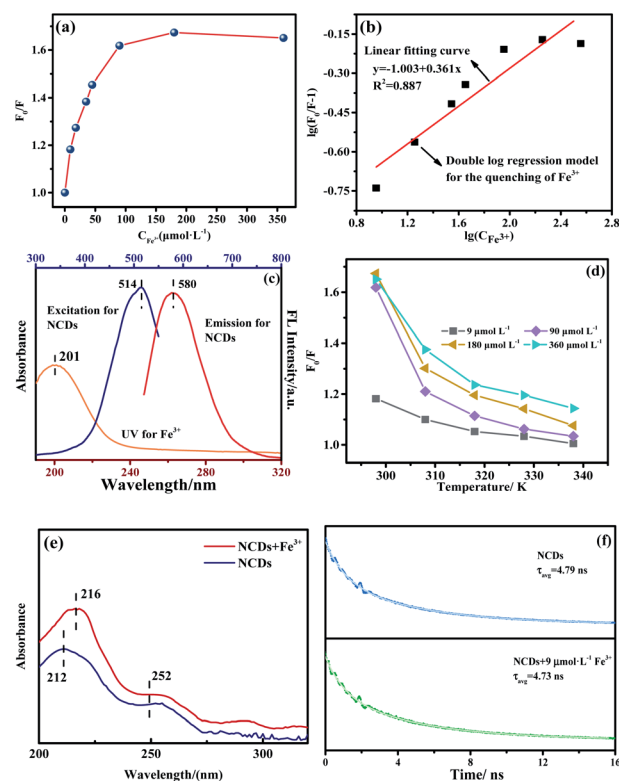

Fig. 7 (a) The relationship of F_0/F versus concentration of Fe^{3+} at 298 K, (b) static fitting of Fe^{3+} quenching for NCDs, (c) UV spectrum of Fe^{3+} and emission and excitation spectra of NCDs, (d) the temperature effect on quenching, (e) the UV-Vis spectra of NCDs and Fe^{3+}-added NCDs, and (f) luminescence decay curves of NCDs with and without adding Fe^{3+} at λ_{ex} = 500 nm and λ_{em} = 580 nm.

effect (IFE).[26–29] The dynamic quenching is triggered by the collision of the quencher ion with the carboxyl, hydroxyl and other functional groups on the surface of NCDs, causing electron transfer. The static quenching is caused by the interaction of the empty orbital of the quencher ion with the π electrons of the NCDs, which can form the complex and results in fluorescence quenching.

Generally, the fluorescence quenching mechanism involves dynamic quenching, static quenching[24,25] and internal filtration effect (IFE).[26–29] Dynamic quenching is triggered by the collision of the quencher ion with the carboxyl, hydroxyl and other functional groups on the surface of NCDs, causing electron transfer. The static quenching is caused by the interaction of the empty orbital in the quencher ion with the π electrons of the NCDs, which can form the complex and results in fluorescence quenching.

The use of eqn (1) for fitting finds that the quenching of NCDs by Fe^{3+} has a large deviation, which indicates that it is not dominated by the dynamic quenching mechanism. When being fitted by the static eqn (2), the values of the related constants of K and n are 0.101 L mol^{-1} and 0.361, respectively, the coefficient R^2 is 0.909. This suggests the static quenching involved. As a matter of fact, it is understandable that the empty virtual orbitals of the Fe^{3+} ion can be filled by the π electrons of the

NCDs on the one hand and oxo groups on the NCDs surface as indicated in XPS (Fig. 4) on the other hand. The IFE mechanism was also explored by using the UV spectrum of Fe^{3+} and the emission and excitation spectra of NCDs (Fig. 7c). One can see that there is no overlap between the Fe^{3+} adsorption and the emission of NCDs. Evidently, this rules out the IFE quenching mechanism.

To prove the postulated static quenching mechanism, we further embarked on several experiments, including the temperature effect on the quenching (Fig. 7d), the absorption spectrum after introducing the quencher (Fig. 7e), and the effect of the quencher on the fluorescence lifetime of the NCDs (Fig. 7f).

According to Fig. 7d, one can see that the relative intensity of F_0/F decreases as the temperature rises. The result indicates that the quench effect reduces once increasing temperature. This is consistent with the static quenching mechanism. In order to verify it, the adsorption spectra of the NCDs and the mixture of NCDs and Fe^{3+} were measured. Fig. 7e displays the difference of adsorption spectra between these two systems, which suggests that NCDs and Fe^{3+} have formed sort of ground-state complex. Moreover, NCDs is rich of π electrons and various oxo functional groups including C=O, C–O, C–OC, O–C=O and OH, which have been evidenced by the XPS spectra of Fig. 4. This provides the essential basis for complexing the iron ion in the mixture solution of NCDs and Fe^{3+}. Focusing on the possibly formed NCDs–Fe complex, the effect of the quencher on the fluorescence lifetime was evaluated. See results of NCDs and Fe^{3+}-added NCDs in Fig. 7f. The determined lifetime of NCDs is 4.79 ns. After adding Fe^{3+}, the lifetime is 4.73 ns. Almost the same lifetime proves that the quenching is dominated by the static mechanism.

Conclusions

High yield of nitrogen-doped carbon dots (NCDs) was prepared by one-step calcination of lignin/melamine formaldehyde foam (LSMF) at 250 °C. The results of SEM, TEM and XRD show that prepared NCDs are uniformly dispersed with a particle size of about 10 nm. Meanwhile, NCDs has high graphitization degree and the surface is rich of functional groups, which would enhance its fluorescence properties. The fluorescence properties and detection for various metal ions were studied, revealing that prepared NCDs have a good identification of Fe^{3+}. The corresponding fluorescence quenching mechanism was postulated as the static quenching. Due to being prepared from the spent foam with a facile method, NCDs would have good application prospect in future.

Experimental

Experimental materials

Sodium lignosulfonate (LS), purchased from Qianjin Welfare Chemical Co., Ltd, Tumen City, Jilin Province; melamine, paraformaldehyde, sodium dodecyl sulfonate, ammonium chloride, triethanolamine, and petroleum ether are purchased from Tianjin Kermel Chemical Reagent Company. All reagents were used as received.

Preparation

Preparation of sodium lignosulfonate melamine formaldehyde (LSMF) foam precursor. 0.3 mol (9.0 g) of para-formaldehyde and 20 mL of deionized water were put in a beaker at 50 °C water bath. After 10 min of stirring, 0.1 mol (about 12.0 g) melamine was added. The pH of mixture was adjusted to 9 by triethanolamine. Then 2.0 g sodium lignosulfonate was added and continue to stir until the solution is clear and transparent.

The mixture was put into the mold. 0.05 g of sodium lauryl sulfate, 4.0 g of ammonium chloride and 5 mL petroleum ether were also put into mold in sequence. After curing in an oven at 80 °C for 24 h, sodium lignosulfonate melamine formaldehyde (LSMF) foam is obtained.

Preparation of N-doped carbon dots (NCDs). The LSMF foam was calcined at a temperature of 250 °C under the protection of N_2 atmosphere. After calcination, the calcined product was dissolved in deionized water and ultrasonically oscillate for 0.5 h. After that, the solution was centrifuge at 8000 rpm for 10 min, then supernatant was collected as obtain N-doped carbon dots (NCDs) aqueous solution. The final NCDs solid was obtained by freeze-dry the aqueous solution. And the 0.1 g freeze-dry NCDs was added to 10 mL deionized water to obtain the NCDs solution.

Characterization

X-ray diffractometer (XRD, D/max-RC, Rigaku, Japan) was applied to characterize the structure of products. The morphology was observed by a scanning electron microscope (SEM, JSM-7500F, JEOL, Japan) and transmission electron microscope (TEM, JEM-2100, JEOL, Japan). The infrared absorption spectra were tested using Fourier transform infrared spectrometer (FT-IR, Frontier type, PerkinElmer, USA). X-ray photoelectron spectroscopy was determined by X-ray photo-electron spectroscopy (XPS, ESCALAB, Thermo, USA).

UV-Vis spectroscopy test

All the UV-Vis spectra were tested with the 3 mL NCDs solution in the two-way quartz cuvette. The ultraviolet-visible spectro-photometer (TU-1950, Beijing Purkinje General Instrument, China) was used.

Fluorescence spectroscopy test

Fluorescence spectrometer (LS 55, PerkinElmer, USA) was used to characterize the fluorescent emission at room temperature (298 K). All the spectra were tested with the 3 mL NCDs solution in the four-way quartz cuvette. The concentration of NCDs is 10 mg mL^{-1}. The excitation light of 500 nm was utilized for NCDs with and without metal ions. The selectivity experiment was performed by adding metal ions including K^+, Na^+, Mg^{2+}, Ca^{2+}, Cr^{3+}, Mn^{2+}, Fe^{3+}, Co^{2+}, Ni^{2+}, Cu^{2+}, Zn^{2+}, Zr^{2+}, Cd^{2+}, Ag^+, Al^{3+} and Pb^{2+}. To make the solution, 3 mL 10 mg mL^{-1} NCDs was

mixed with the 15 μL 90 μmol L^{-1} metal ion solution, followed by 1 min reaction period at room temperature, the fluorescence emission response was recorded in the same condition.

The temperature effect of the Fe^{3+} quenching was carried out at the different temperature (298, 308, 318, 328, 338, and 348 K). NCDs and Fe^{3+} solution were kept at the corresponding temperature for 10 min, and then reacting for 1 min. The fluorescence emission response was recorded under consistent conditions.

The luminescent lifetime and the absolute quantum yield were measured by a photoluminescence spectrometer (Edinburgh Instruments, FLS1000, England). The luminescent lifetime of τ matches with the double exponential function:[30,31]

$$R(t) = B_1 e^{(-t/\tau_1)} + B_2 e^{(-t/\tau_2)} \tag{3}$$

where B_1 and B_2 are the intensity amplitudes at $t = 0$, and τ_1 and τ_2 are the lifetime of each exponential decay.

The average lifetime τ_{avg} is defined as:

$$\tau_{avg} = \frac{B_1 \tau_1^2 + B_2 \tau_2^2}{B_1 \tau_1 + B_2 \tau_2} \tag{4}$$

Conflicts of interest

There are no conflicts to declare.

Acknowledgements

References

1 N.-D. Zhao, Y. Wang, X.-H. Zou, W.-M. Yin, X.-Y. Wang, Y.-R. Guo and Q.-J. Pan, *Chem. Eng. J.*, 2021, **426**, 130812.

2 M. Liu, C. Zhang, Z. Du and W. Zou, *Comp. Interf.*, 2021, **28**, 255–271.

3 X. T. Wang, Y. Shi, Y. Liu and Q. Wang, *J. Polym. Res.*, 2019, **26**, 57–68.

4 H. H. Liao, H. Y. Li, Y. Liu and Q. Wang, *Polym. Int.*, 2019, **68**, 410–417.

5 X. Wang, Z. Han, Y. Liu and Q. Wang, *Appl. Surf. Sci.*, 2020, **505**, 144577–144587.

6 B. Zhang, S. Li, X. Fei, H. Zhao and X. Lou, *Colloids Surf., A*, 2020, **603**, 125219–125225.

7 H. Zhu and S. Xu, *ACS Omega*, 2020, **5**, 9658–9667.

8 B. Song, H. Liang, R. Sun, P. Peng, Y. Jiang and D. She, *Int. J. Biol. Macromol.*, 2020, **144**, 219–230.

9 Y.-H. Chan, Y. Jin, C. Wu and D. T. Chiu, *Chem. Commun.*, 2011, **47**, 2820–2822.

10 E. L. Que, D. W. Domaille and C. J. Chang, *Chem. Rev.*, 2008, **108**, 1517–1549.

11 X. Xu, R. Ray, Y. Gu, H. J. Ploehn, L. Gearheart, K. Raker and S. A. Walter, *J. Am. Chem. Soc.*, 2004, **126**, 12736–12737.

12 M. Lu and L. Zhou, *ACS Omega*, 2019, **101**, 352–359.

13 C. A. Ma, C. S. Yin, Y. J. Fan, X. F. Yang and X. P. Zhou, *J. Mater. Sci.*, 2019, **54**, 9372–9384.

14 W.-M. Yin, Y. Wang, Y.-C. Hou, Y. Sun, J.-G. Zhang, H.-L. Sun, S.-J. Li, Q.-J. Pan and Y.-R. Guo, *Chem. Eng. J.*, 2020, **401**, 125961–125970.

15 H. Qi, M. Teng, M. Liu, S. Liu, J. Li, H. Yu, C. Teng, Z. Huang, H. Liu, Q. Shao, A. Umar, T. Ding, Q. Gao and Z. Guo, *J. Colloid Interface Sci.*, 2019, **539**, 332–341.

16 D. Pan, J. Zhang, Z. Li and M. Wu, *Adv. Mater.*, 2010, **22**, 734–738.

17 L. Li, G. Wu, G. Yang, J. Peng, J. Zhao and J.-J. Zhu, *Nanoscale*, 2013, **5**, 4015–4039.

18 Y. Dong, H. Pang, H. B. Yang, C. Guo, J. Shao, Y. Chi, C. M. Li and T. Yu, *Angew. Chem., Int. Ed.*, 2013, **52**, 7800–7804.

19 M. Saxena and S. Sarkar, *Diamond Relat. Mater.*, 2012, **24**, 11–14.

20 Y.-P. Sun, B. Zhou, Y. Lin, W. Wang, K. A. S. Fernando, P. Pathak, M. J. Meziani, B. A. Harruff, X. Wang, H. Wang, P. G. Luo, H. Yang, M. E. Kose, B. Chen, L. M. Veca and S.-Y. Xie, *J. Am. Chem. Soc.*, 2006, **128**, 7756–7757.

21 Z. Liang, L. Zeng, X. Cao, Q. Wang, X. Wang and R. Sun, *J. Mater. Chem. C*, 2014, **2**, 9760–9766.

22 R. S. A. Sonthanasamy, N. M. N. Sulaiman, L. L. Tan and A. M. Lazim, *Spectrochim. Acta, Part A*, 2019, **218**, 85–96.

23 D. Saha and D. P. S. Negi, *Chem. Phys.*, 2020, **530**, 110644–110649.

24 J. R. Lakowicz, *Principles of fluorescence spectroscopy*, Springer science & business media, 2013.

25 W. Liu, H. Diao, H. Chang, H. Wang, T. Li and W. Wei, *Sens. Actuators, B*, 2017, **241**, 190–198.

26 F. L. Zu, F. Y. Yan, Z. J. Bai, J. X. Xu, Y. Y. Wang, Y. C. Huang and X. G. Zhou, *Microchim. Acta*, 2017, **184**, 1899–1914.

27 H. Liu, C. Xu, Y. Bai, L. Liu, D. Liao, J. Liang, L. Liu and H. Han, *Spectrochim. Acta, Part A*, 2017, **171**, 311–316.

28 T. D. Gauthier, E. C. Shane, W. F. Guerin, W. R. Seitz and C. L. Grant, *Environ. Sci. Technol.*, 1986, **20**, 1162–1166.

29 J. Liu, Y. Chen, W. Wang, J. Feng, M. Liang, S. Ma and X. Chen, *J. Agric. Food Chem.*, 2016, **64**, 371–380.

30 M. Li and P. R. Selvin, *J. Am. Chem. Soc.*, 1995, **117**, 8132–8138.

31 M. Kawa and J. M. J. Fréchet, *Chem. Mater.*, 1998, **10**, 286–296.